

The Measurement of Lightning Environmental Parameters Related to Interaction with Electronic Systems

CARL E. BAUM, SENIOR MEMBER, IEEE, EDWARD L. BREEN, MEMBER, IEEE, FELIX L. PITTS,
GARY D. SOWER, MEMBER, IEEE, AND MITCHEL E. THOMAS

CLEARED
FOR PUBLIC RELEASE
FL/PA 31 DEC 96

Abstract—The measurement of electromagnetic fields and related quantities in a lightning environment is a challenging problem, especially at high frequencies and/or in the immediate vicinity of the lightning arcs and corona. This paper reviews the techniques for accomplishing such measurements in these regimes with examples. These sensors are often the same as for the nuclear electromagnetic pulse (EMP), but significant differences also appear.

Key Words—Electromagnetic sensors, lightning, aircraft applications.

I. INTRODUCTION

THE MEASUREMENT of electromagnetic-field parameters is at once both simple and complex. From one point of view one need only make an elementary application of the Maxwell equations. The resulting quasi-static concepts give some basic design approaches for electromagnetic-field sensors. However, this is only the beginning; things are not as simple as they may first seem. A more sophisticated point of view recognizes that numerous complications cloud such a picture. One exception relates to the limitations of quasi-static theory; one often wants the maximum sensitivity (and corresponding size). Another exception relates to the complexity of environmental conditions in which the electromagnetic fields are accompanied by other electromagnetic parameters such as source currents, nonlinear conductivities, etc., which are not present under the classical assumptions concerning field measurements. Both of these exceptions are sometimes encountered in lightning electromagnetic measurements.

Lightning electromagnetic measurements have some similarity to electromagnetic measurements under other conditions. Much of the technology discussed here has evolved initially through the nuclear electromagnetic pulse (EMP) program. EMP environmental measurements include cases in which a large bandwidth is desired and cases in which source region considerations are important (including nuclear radiation, source current density, and nonlinear and time-varying air conductivity). The sensor designs for EMP measurements have been discussed in a previous extensive review paper with numerous references [1]. While there are some differ-

ences in the case of lightning, many of the design considerations are the same or similar.

Another application of electromagnetic sensors is in pulse-power generators where large impulsive voltages and currents and associated electromagnetic fields are present. Such pulse-power equipment finds application in nuclear and lightning environmental simulation (among various applications). The design techniques for electromagnetic sensors have been applied here as well, both for large bandwidth and for source-region problems (as in associated charged-particle beams). Another recent review paper considers this application of such sensors, including topology and symmetry considerations for the installation of such sensors and the associated instrumentation cabling in the experimental geometries [3].

In the lightning context such sensors together with the techniques for installing them into instrumentation systems have application for determining the fast-transient character of the electromagnetic fields both away from lightning strokes and on objects under direct strike conditions [2]. Such applications are reviewed and updated here.

The kind of sensors we are discussing are not typical antennas as thought of by most people. In the past (as well as present) much attention has been devoted to antennas for communication and radar; these now have a large literature. When one designs an antenna he usually has some kind of application in mind. While the basic concept of electrically-small antennas has been around for a while, it has only been in recent years (about the last two decades) that there has been a serious effort to optimize the designs of such special antennas into what we term sensors [1]. This optimization for electromagnetic measurements includes accuracy, sensitivity, bandwidth, and broadband/transient performance. The problems here become especially difficult when one includes the design of such sensors for use in severe environments involving sources and/or nonlinear and time varying conductivity. Later sections discuss such design problems.

Past lightning measurements have often been characterized by slower response times (small bandwidths), often due to limited recorder bandwidth. In such cases the bandwidth of the sensors including the effects of nearby scatterers were often not significant. Appleton *et al.* [4] in 1923 and Norinder [5] in 1937 are examples of early electromagnetic measurements of this type. Of more recent vintage, several papers typify some advances in this art [6]-[12]. These measurements have been advanced in bandwidth by Weidman

Manuscript received November 13, 1981.

C. E. Baum and E. L. Breen are with the Air Force Weapons Lab., Kirtland Airforce Base, NM 87117. (505) 844-9816.

F. L. Pitts and M. E. Thomas are with NASA Langley Research Center, Hampton, VA 23665.

G. D. Sower is with EG&G Alamo Ave. SE, Albuquerque, NM 87106.

Note 274

Measurement of Lightning Environmental Parameters Related to Interaction with Electronic Systems

CARL E. BAUM, SENIOR MEMBER, IEEE, EDWARD L. BREEN, MEMBER, IEEE, FELIX L. PITTS,
GARY D. SOWER, MEMBER, IEEE, AND MITCHEL E. THOMAS

The measurement of electromagnetic fields and related parameters in a lightning environment is a challenging problem, especially at high frequencies and/or in the immediate vicinity of the lightning strokes and corona. This paper reviews the techniques for making such measurements in these regimes with examples. The techniques are often the same as for the nuclear electromagnetic pulse (EMP), but significant differences also appear.

Keywords—Electromagnetic sensors, lightning, aircraft applications.

I. INTRODUCTION

MEASUREMENT of electromagnetic-field parameters can be either once both simple and complex. From one point of view, one need only make an elementary application of the basic equations. The resulting quasi-static concepts give simple design approaches for electromagnetic-field sensors. However, this is only the beginning; things are not as simple as they may first seem. A more sophisticated point of view reveals that numerous complications cloud such a picture. One relates to the limitations of quasi-static theory. One often wants the maximum sensitivity (and correspondingly the minimum size). Another exception relates to the complexity of the environmental conditions in which the electromagnetic measurements are accompanied by other electromagnetic parameters such as source currents, nonlinear conductivities, etc., which are not present under the classical assumptions concerning electromagnetic measurements. Both of these exceptions are sometimes encountered in lightning electromagnetic measurements.

Lightning electromagnetic measurements have some similarities to electromagnetic measurements under other conditions. Much of the technology discussed here has evolved through the nuclear electromagnetic pulse (EMP) environment. EMP environmental measurements include cases in which a large bandwidth is desired and cases in which source current density, and nonlinear and time-varying characteristics are important (including nuclear radiation activity). The sensor designs for EMP measurements are discussed in a previous extensive review paper [1]. While there are some differences

in the case of lightning, many of the design considerations are the same or similar.

Another application of electromagnetic sensors is in pulse-power generators where large impulsive voltages and currents and associated electromagnetic fields are present. Such pulse-power equipment finds application in nuclear and lightning environmental simulation (among various applications). The design techniques for electromagnetic sensors have been applied here as well, both for large bandwidth and for source-region problems (as in associated charged-particle beams). Another recent review paper considers this application of such sensors, including topology and symmetry considerations for the installation of such sensors and the associated instrumentation cabling in the experimental geometries [3].

In the lightning context such sensors together with the techniques for installing them into instrumentation systems have application for determining the fast-transient character of the electromagnetic fields both away from lightning strokes and on objects under direct strike conditions [2]. Such applications are reviewed and updated here.

The kind of sensors we are discussing are not typical antennas as thought of by most people. In the past (as well as present) much attention has been devoted to antennas for communication and radar; these now have a large literature. When one designs an antenna he usually has some kind of application in mind. While the basic concept of electrically small antennas has been around for a while, it has only been in recent years (about the last two decades) that there has been a serious effort to optimize the designs of such special antennas into what we term sensors [1]. This optimization for electromagnetic measurements includes accuracy, sensitivity, bandwidth, and broadband/transient performance. The problems here become especially difficult when one includes the design of such sensors for use in severe environments involving sources and/or nonlinear and time varying conductivity. Later sections discuss such design problems.

Past lightning measurements have often been characterized by slower response times (small bandwidths), often due to limited recorder bandwidth. In such cases the bandwidth of the sensors including the effects of nearby scatterers were often not significant. Appleton *et al.* [4] in 1923 and Norinder [5] in 1937 are examples of early electromagnetic measurements of this type. Of more recent vintage, several papers typify some advances in this art [6]–[12]. These measurements have been advanced in bandwidth by Weidman

Manuscript received November 13, 1981.

Carl E. Baum and E. L. Breen are with the Air Force Weapons Lab., Kirtland Air Force Base, NM 87117. (505) 844-9816.

Felix L. Pitts and M. E. Thomas are with NASA Langley Research Center, Hampton, VA 23665.

Edward L. Breen is with EG&G Alamo Ave. SE, Albuquerque, NM 87106.

Note 274

The Measurement of Lightning Environmental Parameters Related to Interaction with Electronic Systems

CARL E. BAUM, SENIOR MEMBER, IEEE, EDWARD L. BREEN, MEMBER, IEEE, FELIX L. PITTS,
GARY D. SOWER, MEMBER, IEEE, AND MITCHEL E. THOMAS

Abstract—The measurement of electromagnetic fields and related quantities in a lightning environment is a challenging problem, especially at high frequencies and/or in the immediate vicinity of the lightning arcs and corona. This paper reviews the techniques for accomplishing such measurements in these regimes with examples. These sensors are often the same as for the nuclear electromagnetic pulse (EMP), but significant differences also appear.

Key Words—Electromagnetic sensors, lightning, aircraft applications.

I. INTRODUCTION

THE MEASUREMENT of electromagnetic-field parameters is at once both simple and complex. From one point of view one need only make an elementary application of the Maxwell equations. The resulting quasi-static concepts give some basic design approaches for electromagnetic-field sensors. However, this is only the beginning; things are not as simple as they may first seem. A more sophisticated point of view recognizes that numerous complications cloud such a picture. One exception relates to the limitations of quasi-static theory; one often wants the maximum sensitivity (and corresponding size). Another exception relates to the complexity of environmental conditions in which the electromagnetic fields are accompanied by other electromagnetic parameters such as source currents, nonlinear conductivities, etc., which are not present under the classical assumptions concerning field measurements. Both of these exceptions are sometimes encountered in lightning electromagnetic measurements.

Lightning electromagnetic measurements have some similarity to electromagnetic measurements under other conditions. Much of the technology discussed here has evolved initially through the nuclear electromagnetic pulse (EMP) program. EMP environmental measurements include cases in which a large bandwidth is desired and cases in which source region considerations are important (including nuclear radiation, source current density, and nonlinear and time-varying air conductivity). The sensor designs for EMP measurements have been discussed in a previous extensive review paper with numerous references [1]. While there are some differ-

ences in the case of lightning, many of the design considerations are the same or similar.

Another application of electromagnetic sensors is in pulse-power generators where large impulsive voltages and currents and associated electromagnetic fields are present. Such pulse-power equipment finds application in nuclear and lightning environmental simulation (among various applications). The design techniques for electromagnetic sensors have been applied here as well, both for large bandwidth and for source-region problems (as in associated charged-particle beams). Another recent review paper considers this application of such sensors, including topology and symmetry considerations for the installation of such sensors and the associated instrumentation cabling in the experimental geometries [3].

In the lightning context such sensors together with the techniques for installing them into instrumentation systems have application for determining the fast-transient character of the electromagnetic fields both away from lightning strokes and on objects under direct strike conditions [2]. Such applications are reviewed and updated here.

The kind of sensors we are discussing are not typical antennas as thought of by most people. In the past (as well as present) much attention has been devoted to antennas for communication and radar; these now have a large literature. When one designs an antenna he usually has some kind of application in mind. While the basic concept of electrically-small antennas has been around for a while, it has only been in recent years (about the last two decades) that there has been a serious effort to optimize the designs of such special antennas into what we term sensors [1]. This optimization for electromagnetic measurements includes accuracy, sensitivity, bandwidth, and broadband/transient performance. The problems here become especially difficult when one includes the design of such sensors for use in severe environments involving sources and/or nonlinear and time varying conductivity. Later sections discuss such design problems.

Past lightning measurements have often been characterized by slower response times (small bandwidths), often due to limited recorder bandwidth. In such cases the bandwidth of the sensors including the effects of nearby scatterers were often not significant. Appleton *et al.* [4] in 1923 and Norinder [5] in 1937 are examples of early electromagnetic measurements of this type. Of more recent vintage, several papers typify some advances in this art [6]–[12]. These measurements have been advanced in bandwidth by Weidman

Manuscript received November 13, 1981.

C. E. Baum and E. L. Breen are with the Air Force Weapons Lab., Kirtland Air Force Base, NM 87117. (505) 844-9816.

F. L. Pitts and M. E. Thomas are with NASA Langley Research Center, Hampton, VA 23665.

G. D. Sower is with EG&G Alamo Ave. SE, Albuquerque, NM 87106.

and Krider [13]; the limitation in bandwidth is not precisely known, but is limited by the geometry of the measurement platform which limits the time resolution to the rough order of 30 ns [14]. This can be compared to the resolution (using EMP techniques) of about 5 ns for the chosen sensors, with negligible distortion due to the measurement platform and 10 ns sample intervals for the digital recording [15]; considerably higher bandwidths are possible using such techniques if desired [1].

II. SOME BASICS

Summarizing some of the basic aspects of electromagnetic sensor design [1], first we have our definition of a sensor as a special kind of antenna with the following properties.

- 1) It is an analog device which converts the electromagnetic quantity of interest to a voltage or current (in the circuit sense) at some terminal pair for driving a load impedance, usually a constant resistance appropriate to a transmission line (cable) terminated in its characteristic impedance.
- 2) It is passive.
- 3) It is a primary standard in the sense that, for converting fields to voltage and current, its sensitivity is well known in terms of its geometry; i.e., it is "calibratable by a ruler." The impedances of loading elements may be measured and trimmed. Viewed another way, it is in principle as accurate as the standard field (voltage, etc.) in a calibration facility. (A few percent accuracy is usually easily attainable in this sense.)
- 4) It is designed to have a specific convenient sensitivity (e.g., $1.00 \times 10^{-3} \text{m}^2$) for its transfer function.
- 5) Its transfer function is designed to be simple across a wide frequency band. This may mean "flat" in the sense of volts per unit field or time derivative of field, or it may mean some other simple mathematical form that can be specified with a few constants (in which case more than one specific convenient sensitivity number is chosen).

A first important category of such sensors is the electric-field sensor. Fig. 1 shows the basic topology of such a sensor (two separate conductors connected to a terminal pair) and its equivalent-circuit representation (valid for electrically small sensors). The three basic sensor parameters are related as

$$\vec{A}_{e_{eq}} = \frac{C}{\epsilon} \vec{l}_{e_{eq}}$$

$$\vec{A}_{e_{eq}} \equiv \text{equivalent area}$$

$$\vec{l}_{e_{eq}} \equiv \text{equivalent length (or height)}$$

$$C \equiv \text{capacitance} \tag{2.1}$$

so that only two of the basic parameters are independent. Note that if in addition to the medium permittivity ϵ there is a conductivity σ , then a conductance G appears in parallel with the capacitance C in the equivalent circuit.

The basic parameters of the magnetic-field sensors are indicated in Fig. 2. The basic topology of such a sensor is a loop broken to connect to a terminal pair. The basic sensor

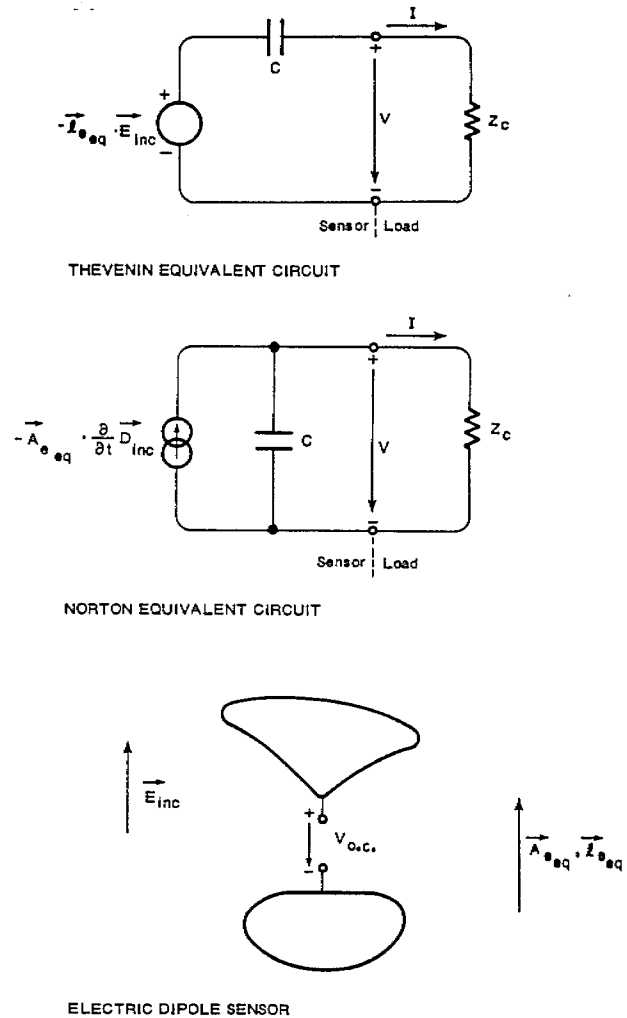


Fig. 1. Electrically small electric-dipole sensor in free space.

parameters are related as

$$\vec{A}_{h_{eq}} = \frac{L}{h} \vec{l}_{h_{eq}}$$

$$\vec{A}_{h_{eq}} \equiv \text{equivalent area}$$

$$\vec{l}_{h_{eq}} \equiv \text{equivalent length}$$

$$L \equiv \text{inductance.} \tag{2.2}$$

Again only two of the basic parameters are independent. The medium permeability μ is often that of free space, μ_0 .

An important question relating to these kinds of sensors is which type is best for a certain kind of application. Such questions are usually cast into an efficiency format in the sense of most output per unit input. Here one must recognize the broad-band character of the measurement problem so that output should also include an appropriate bandwidth in its definition.

One concept of historical and technical interest is that of equivalent volume that has the formulas for electric and mag-

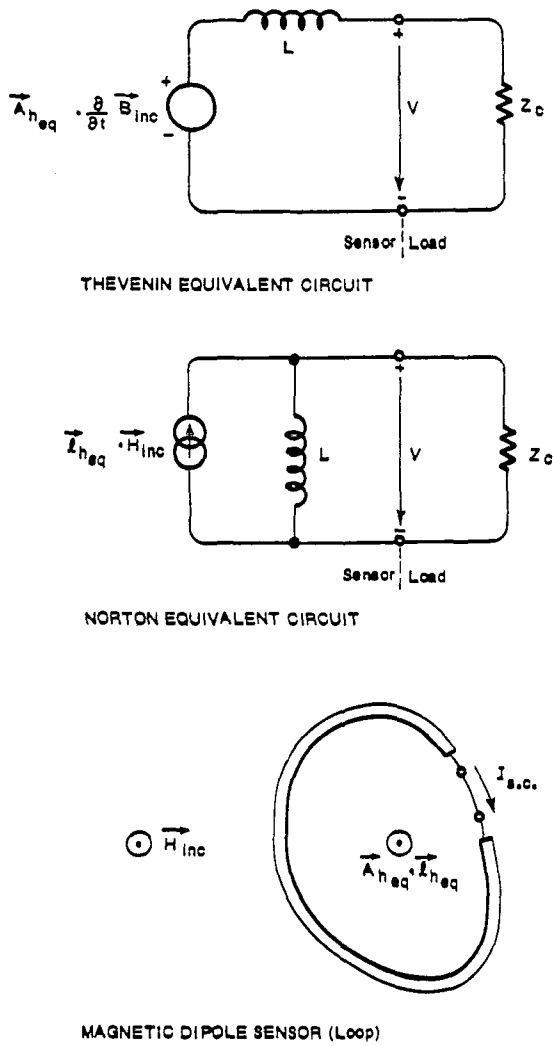


Fig. 2. Electrically small magnetic-dipole sensor in free space.

netic dipole sensors, respectively

$$\begin{aligned}
 V_{eeq} &= \frac{\epsilon_0}{C} \vec{A}_{eeq} \cdot \vec{A}_{eeq} \\
 &= \frac{C}{\epsilon_0} \vec{l}_{eeq} \cdot \vec{l}_{eeq} \\
 &= \vec{A}_{eeq} \cdot \vec{l}_{eeq} \\
 V_{heq} &= \frac{\mu_0}{L} \vec{A}_{heq} \cdot \vec{A}_{heq} \\
 &= \frac{L}{\mu_0} \vec{l}_{heq} \cdot \vec{l}_{heq} \\
 &= \vec{A}_{heq} \cdot \vec{l}_{heq}.
 \end{aligned} \tag{2.3}$$

The equivalent volume is based on the energy extracted from the incident field and delivered to the load. This equivalent volume can be divided by the geometrical volume to give a dimensionless efficiency. This geometrical volume might be

a specified volume into which the sensor is to fit; the better sensor design has the better efficiency. This type of definition is appropriate for cases in which the critical frequency $1/(Z_c C)$ and Z_c/L (for constant resistance Z_c) is within the electrically small regime, and the basic limitation on the sensor design is size.

Several of the sensor types discussed herein are not constrained directly by physical dimensions but by upper frequency response (f_c which might be interpreted as a characteristic time t_c , or length l_c) for which the approximation of the response being proportional to the time derivative type of field quantity dotted into an equivalent area breaks down. The sensor size can be made as large as possible to obtain sensitivity for a given bandwidth. As the sensor size is increased, the approximation of an electrically small sensor breaks down at the highest frequencies of interest. One defines then the characteristic frequency or time according to when the ideal dot product and derivative response is in error by some specified amount. The resulting figure of merit is found to be

$$\begin{aligned}
 \Lambda_e &= \left(\frac{Z_c}{Z_0} \right)^{1/2} |\vec{A}_{eeq}| l_c^{-2} \\
 \Lambda_h &= \left(\frac{Z_0}{Z_c} \right)^{1/2} |\vec{A}_{heq}| l_c^{-2}
 \end{aligned} \tag{2.4}$$

for electric and magnetic dipole sensors, respectively, where the wave impedance of free space is

$$Z_0 = \left(\frac{\mu_0}{\epsilon_0} \right)^{1/2} \tag{2.5}$$

and Z_c is the assumed frequency-independent load resistance, typically the characteristic impedance of a transmission line. For this purpose, we have introduced a characteristic length (noting that the high-frequency limitation tends to be related to transit times on the structure) as

$$l_c = ct_c = \frac{c}{\omega_c} \tag{2.6}$$

where c is the speed of light, thus putting the bandwidth in length units. The figure of merit is of the form sensitivity times (bandwidth)², a quantity which is not a function of sensor size but only a function of the design, shape, and impedance loading distribution. The definition of this figure of merit is based on power delivered to the load Z_c which places electric and magnetic sensors on a common basis for comparison. Note that, in this form, the figure of merit applies to sensors in free space (or uniform isotropic media). In this paper, the figures of merit quoted are based on a 10 to 90 percent rise time of the output waveform to a ramp or step input waveform as appropriate and designated as Λ_{10-90} .

The various sensors in their free-space designs can usually be mounted on ground planes by cutting them in half along an appropriate symmetry plane. The figures of merit for a

given type of design are different in these two situations. In this paper we refer the figures of merit for each design type to their free-space (full sensor) versions. Note that a particular sensor design in a ground plane version may have a different equivalent area and drive a different load impedance, although both are simply related to the free-space versions.

Current sensors are a special category. An important class relies on an integral form of one of Maxwell's equations as

$$\oint_C \vec{H} \cdot d\vec{l} = \int_S \vec{J}_t \cdot d\vec{S} \equiv I_t \quad (2.7)$$

where \vec{J}_t is the total current density passing through the surface S bounded by the contour C . As indicated in Fig. 3, the basic sensor concept is to measure the magnetic field (or usually its time derivative) at many places around an area through which the current of interest flows. Appropriately summing (or averaging) these measurements experimentally gives the total current through the area. Note that the total current density is just

$$\vec{J}_t = \nabla \times \vec{H} = \vec{J}_c + \vec{J}_\sigma + \vec{J}_e \quad (2.8)$$

including source current density \vec{J}_c (e.g., the Compton current density in an EMP source region), and the conduction (\vec{J}_σ) and displacement (\vec{J}_e) current densities which may be even non-linear in some circumstances. In linear, time-invariant, isotropic media we have

$$\vec{J}_t = \vec{J}_c + \sigma \vec{E} + \frac{\partial}{\partial t} \vec{D} \quad (2.9)$$

$$\vec{D} = \epsilon \vec{E}.$$

Voltage sensors are closely associated with electric-field sensors. Electric-field sensors typically measure the potential (voltage) between two conductors (highly conducting compared to the total medium conductivity) and relate this potential to the electric field through an equivalent length as in (2.1). Here we need only the potential difference itself. However, like an electric-field sensor, voltage sensors have bandwidth restrictions related to the definition of potential. As in Fig. 4, one has the voltage as a path integral of the electric field as

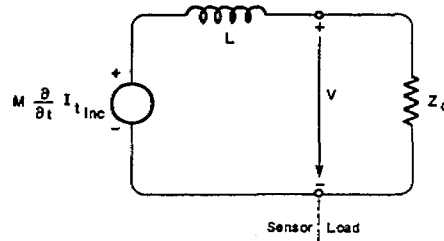
$$V = - \int_C \vec{E} \cdot d\vec{l} \quad (2.10)$$

where C connects points \vec{r}_1 and \vec{r}_2 on two separate conductors. However

$$\vec{E} = -\nabla\Phi - \frac{\partial}{\partial t} \vec{A}$$

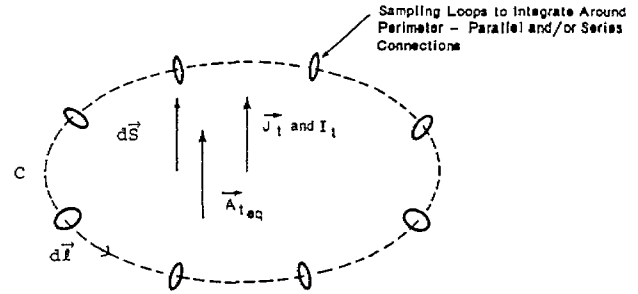
$\Phi \equiv$ scalar potential

$$\vec{A} \equiv \text{vector potential} \quad (2.11)$$



$$I_{t,inc} = \vec{A}_{t,eq} \cdot \vec{J}_{t,inc} \quad \text{For Measurement of Distributed Current Density}$$

NORTON EQUIVALENT CIRCUIT



Approximate Integration Pattern - Approximate Perimeter for Equivalent Area for Total Current Density

INDUCTIVE CURRENT SENSOR (Multiple Loops)

Fig. 3. Electrically small inductive-current sensor in free space.

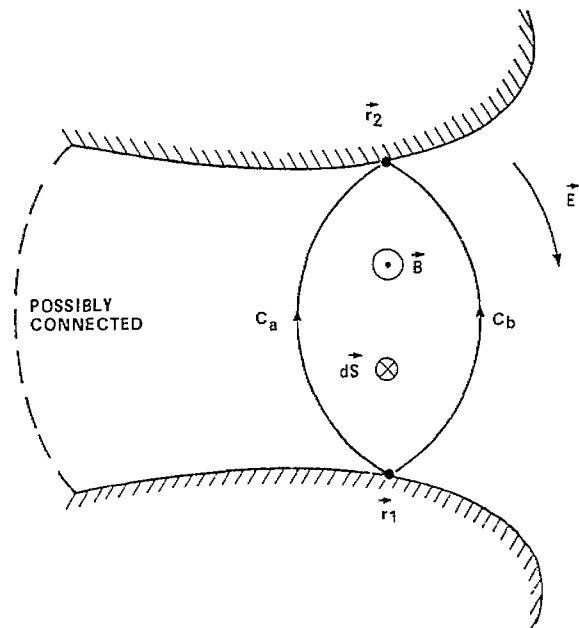


Fig. 4. Voltage sensor definition.

giving (for stationary C)

$$\begin{aligned} V &= \int_C (\dots) \cdot d\vec{l} + \frac{\partial}{\partial t} \int_C \vec{A} \cdot d\vec{l} \\ &= [\Phi(\vec{r}_2) - \Phi(\vec{r}_1)] + \frac{\partial}{\partial t} \int_C \vec{A} \cdot d\vec{l} \end{aligned} \quad (2.12)$$

Now, if one has more than one possible contour, say C_a and C_b , then the corresponding voltages, V_a and V_b , are in general different as

$$\begin{aligned}
 V_a - V_b &= - \int_{C_a} \vec{E} \cdot d\vec{l} + \int_{C_b} \vec{E} \cdot d\vec{l} \\
 &= - \int_{C_a - C_b} \vec{E} \cdot d\vec{l} \\
 &= \frac{\partial}{\partial t} \int_{C_a - C_b} \vec{A} \cdot d\vec{l} \\
 &= \frac{\partial}{\partial t} \int_{S_{a,b}} \vec{B} \cdot d\vec{S}
 \end{aligned} \tag{2.13}$$

$S_{a,b}$ = surface bounded by contour $C_a - C_b$

which is derived from either of

$$\begin{aligned}
 \nabla \times \vec{E} &= - \frac{\partial}{\partial t} \vec{B} \quad (\vec{B} = \mu \vec{H}) \\
 \vec{B} &= \nabla \times \vec{A}.
 \end{aligned} \tag{2.14}$$

Typically the contour of concern is near some electrical connection. However, one must be careful (at high frequencies especially) of regarding conductors as equipotentials for voltage measurements. Note that this definition even allows for the measurement of the voltage between two points on the same conductor (e.g., a loop) when $\Phi_a = \Phi_b$.

For more detail concerning these points see [1]-[3] and their references.

III. SENSORS FOR USE AWAY FROM LIGHTNING ARCS AND CORONA

Electromagnetic sensors for use in measuring lightning phenomena at a distance sufficiently removed from the lightning stroke that arcs and corona are not present are very similar to sensors used for EMP measurements away from a nuclear source region. These sensors may be used in one of two ways, for measurement of the environment created by the lightning and for measurement of the response of a system to the environmental fields. The reader may consult the references of [1] for many more details.

A. D-dot and E-Field Sensors

The D-dot sensor is used to measure the time rate of change of electric flux density. The sensor's response is described by the Norton equivalent circuit of Fig. 1. The frequency-domain response of the sensor is given, for bandwidth limited by capacitance and not by transit times, by

$$\tilde{V}(s) = \frac{es\vec{E}_{inc}(s) \cdot \vec{A}_{eeq} Z_c}{1 + sZ_c C} \tag{3.1}$$

and for frequencies where $\omega \ll 1/(Z_c C)$ the response can be



Fig. 5. Photo of HSD-S1A(R).

simply expressed as

$$\tilde{V}(s) = es\vec{E}_{inc}(s) \cdot \vec{A}_{eeq} Z_c. \tag{3.2}$$

It is of primary importance that an accurate determination of sensor equivalent area can be made. For that reason, only sensor geometries with accurately calculable equivalent areas are used. Sensor capacitance as a design parameter need not be known so accurately, but it should be a low value as it shunts the load resistance and determines the high-frequency response. For very fast sensors, it should be small enough that the high-frequency response is determined by transit-time effects.

1) *Hollow Spherical Dipole (HSD)*: The HSD sensor design uses the geometry of a sphere with a narrow slot around the equator. The slot is resistively loaded by the signal cables. The sensor shown in Fig. 5 is the HSD-S1A(R) for use on a conducting ground plane. Signal current from the hemispherical shell flows to the ground plate through the 50- Ω coaxial cable output impedance. The HSD-2A(R) is a balanced-output version of the sensor for free-space measurements; the signals from the two hemispheres produce a differential signal which is produced at the 100- Ω twinaxial connector. The sensitivity of the HSD sensor is expressed as an equivalent area. The area is shown to be $A_{eeq} = 3\pi a^2$ where a is the sensor sphere radius. The Λ_{10-90} figure of merit for this sensor is 0.078. HSD sensors have been fabricated with equivalent areas of 0.1 and 0.01 m² in both differential and single-ended versions.

2) *Asymptotic Conical Dipole (ACD)*: An improved sensor geometry from the standpoint of figure of merit is the ACD. The particular shape used to date is derived from a line charge $\lambda(z)$ on the z axis given by

$$\lambda(z) = \begin{cases} \lambda_0, & \text{for } 0 < z < z_0 \\ -\lambda_0, & \text{for } 0 > z > -z_0 \\ 0, & \text{for } z = 0 \\ 0, & \text{for } |z| > z_0 \end{cases} \tag{3.3}$$

$$(\lambda_0 > 0, z_0 > 0).$$

The potential distribution for the above charge distribution



Fig. 6. ACD-5A(A) D-dot sensor.

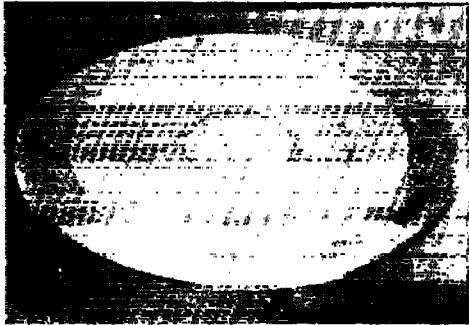


Fig. 7. Flush-plate-dipole D-dot sensor.

is solved for the electrostatic equipotentials surrounding it. The surface of the sensor corresponds to that particular equipotential surface which is asymptotic to a 100- Ω bicone at its apex (in the differential form). The ACD-5A(A) sensor is shown in Fig. 6. It consists of the sensor element attached to a 50- Ω coaxial cable which passes within the ground plane to the output connector. The sensor element is supported by a thin dielectric cylinder which provides weather protection and mechanical support. The sensor has an equivalent area of 1 m² and an upper frequency response >75 MHz. Sensor element capacitance to ground is 17 pF. The corresponding Λ_{10-90} figure of merit is >0.3 related to a differential configuration which is comparable to the MGL B-dot sensors. The ACD sensors have also been fabricated with equivalent areas of 10^{-1} through 10^{-4} m² in both differential and single-ended versions for far-field lightning measurements.

3) *Flush-Plate Dipole (FPD)*: The geometries of the HSD and ACD sensors cause electric-field enhancement which is most pronounced at the top of the sensing element. The FPD minimizes field enhancement and chances for field distortion on test objects. The sensor geometry is shown in Fig. 7. It is basically a conducting disk centered in a circular aperture in a conducting ground plane. The signal is taken from the sensor element at its circumference by signal paths which are paralleled into a 50- Ω connector. The flat surface of the sensor is protected by a weather cover. The bottom side of the sensor is covered by a conducting pan to provide a consistent electrical environment as well as to provide protection. The equivalent area of the FPD is derived in a form in which the area is given as a normalized area $A = |A_{eq}|/(\pi ab)$ and where a and b are the radii of the sensor element and the circular

aperture, respectively. For the FPD-1A the sensitivity $A_{eq} = 0.01$ m². The normalized capacitance is calculated for various disk and aperture radii, and for the dimensions of the FPD-1A that value is 6.8 pF. This value of capacitance along with the 50- Ω cable impedance would give a frequency response of 468 MHz. The presence of the mylar sheet covering the sensor, the disk support structure, and the bottom cover add an additional 1.2 pF and reduce the frequency response to approximately 390 MHz. The Λ_{10-90} figure of merit is 0.08 related to a differential configuration.

4) *Parallel-Plate Dipole (PPD)*: An electric-field sensor uses the case $\omega \gg 1/(Z_c C)$ in (2.1) giving the equivalent length (or height) as the appropriate sensitivity parameter. Various versions of this have been used. Its disadvantage lies in the attenuation introduced by added series resistance to increase the effective value of Z_c . Of course, one can consider active versions of this device.

B. B-dot and H-Field Sensors

The transfer function of the magnetic-field sensor of Fig. 2 is given by

$$\tilde{V}(s) = \frac{s\vec{B}_{inc}(s) \cdot \vec{A}_{neq} Z_c}{sL + Z_c} \quad (3.4)$$

For frequencies where $\omega \ll Z_c/L$, we have the derivative response

$$\tilde{V}(s) = s\vec{B}_{inc}(s) \cdot \vec{A}_{neq} \quad (3.5)$$

For frequencies where $\omega \gg Z_c/L$, we have the self-integrating response where we have used the concept of equivalent length:

$$\tilde{V}(s) = \vec{H}_{inc}(s) \cdot \vec{l}_{neq} Z_c \quad (3.6)$$

1) *Multigap Loop (MGL)*: The MGL series of magnetic-field sensor is used for high-frequency B-dot measurements. The basic free-field MGL (full-loop) sensor is built in the form of a right circular cylinder. The conducting cylinder is formed from printed-circuit-board material which is etched to provide the gaps and signal pick-off points. The sensor is divided into four quadrants by axial shorting plates that connect to the cylinder midway between the gaps. The signals from quadrants one and three are combined to form one side of the differential output signal, and the signals from quadrants two and four are combined to form the other. Combining the signals in this manner minimizes the E-field and other higher-order error responses. The cylindrical geometry of the MGL sensor permits an approximate determination of the effects of the number of gaps, the cable impedance, the sensor length, and orientation of the gaps with respect to the magnetic field. The single-ended sensors are essentially one-half of the sensor described above, except that they consist of two adjacent quadrants with signals connected in parallel. The MGL-3A (10^{-1} m²) used for far-field lightning measurements is shown in Fig. 8. MGL sensors have been built with equivalent areas of 10^{-1} through 10^{-5} m². Equivalent area is maintained to an accuracy of ± 3 percent. The Λ_{10-90} figure of merit is 0.24.



Fig. 8. MGL-3A *B*-dot sensor.

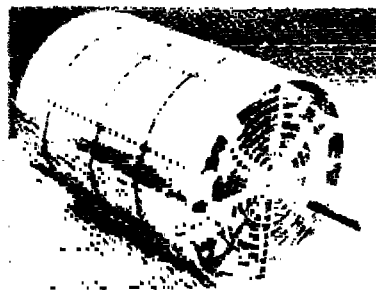


Fig. 10. MTL-1 sensor (coil with axial shorts and conducting shield in place).

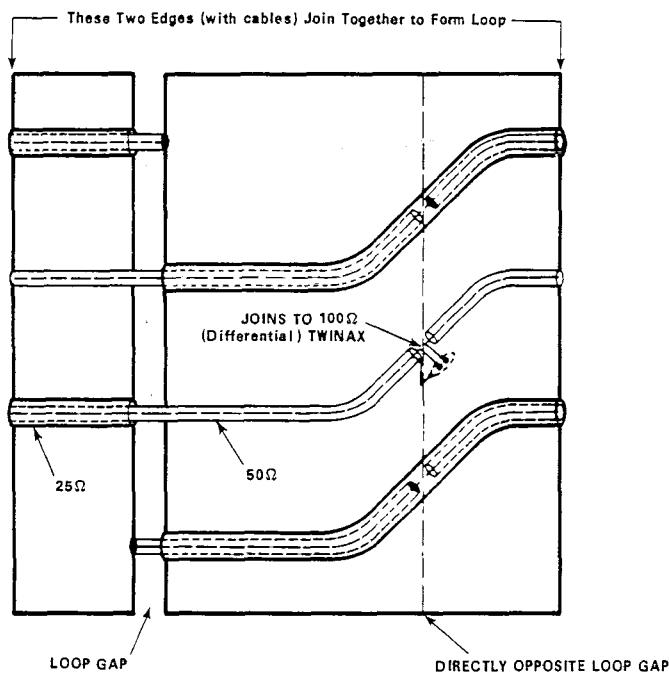


Fig. 9. OML-1A (A) *B*-dot loop sensor (expanded diagram).

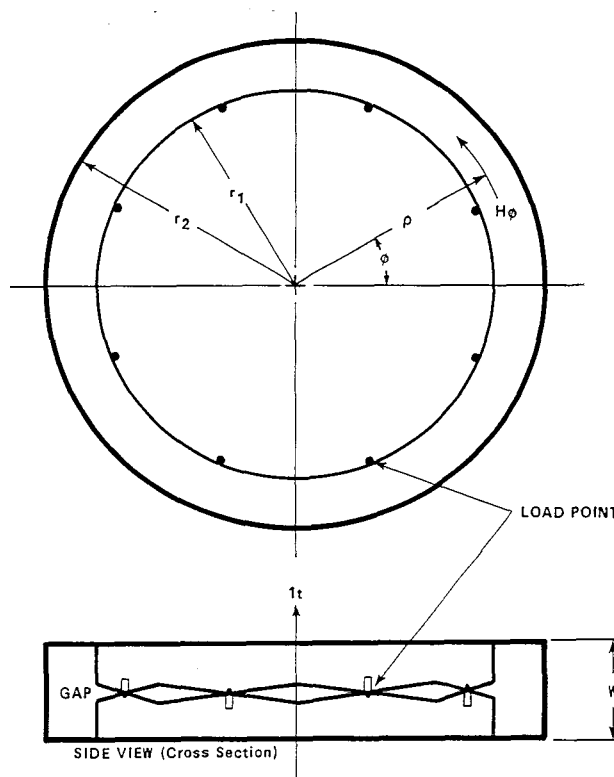


Fig. 11. Typical CPM sensor geometry.

2) *One-Conductor, Many-Turn Loop (OML)*: A single-gap half-cylinder loop with four-turn wiring and an equivalent area of 1 m^2 is available for measurements requiring more sensitivity. This sensor, designated the OML-1A(A), operates as a derivative output device at frequencies below 3.5 MHz and has a risetime of about 100 ns. Fig. 9 shows this sensor. Special triaxial cable with $25\text{-}\Omega$ outer line and $50\text{-}\Omega$ inner line is used. The gap voltage is picked off at four points and carried by the $25\text{-}\Omega$ outer lines to two summing gaps in the $50\text{-}\Omega$ internal lines. The two $50\text{-}\Omega$ lines drive the $100\text{-}\Omega$ differential output at the final gap in the cable. The four voltage pickoff points along the gap were selected experimentally to optimize frequency response.

3) *Multiturn Loop (MTL)*: The MTL-1 is a full-loop (free field) 50-turn sensor with an equivalent area of 10 m^2 and a *B*-dot upper frequency response of approximately 25 kHz. Above 25 kHz, the sensor is self-integrating with its useful bandwidth extending to 3 MHz. Above this frequency, resonances within the complex signal-distribution network perturb the output signal. The sensor has an equivalent length of 0.02 m. The MTL-1 design employs several special features to achieve the 3-MHz bandwidth [1], [2]. It has four loop-gap

signal pickoffs and is wound in two identical 25-turn half-loops, each of which drives one side of the differential output. Fig. 10 shows the sensor interior. The quotient of equivalent volume divided by geometric volume is 1.3.

The MTL-2 has ten turns, an equivalent area of 10^{-2} m^2 , an equivalent length of 10^{-2} m , a self-inductance of $1.25 \times 10^{-6} \text{ H}$, and an upper frequency response of 12.6 MHz for *B*-dot operation. The quotient of equivalent volume divided by geometric volume is 0.56.

C. Current and Current-Density Sensors

1) *Circular Parallel Mutual-Inductance Sensor (CPM)*: This sensor is used to measure the time derivative of the total current through the aperture of the sensor. The CPM is an inductive sensor of toroidal shape as illustrated in Fig. 11. The loop turns are oriented to be sensitive to the ϕ component of the magnetic field H with respect to the measurement axis. This sensor has a cross section of width w , an inner radius r_1 ,



Fig. 12. Instrumentation room (Kiva) and electromagnetic-field sensors.

and an outer radius r_2 . The mutual inductance is

$$M = \frac{N\mu_r\mu_0 w \ln\left(\frac{r_2}{r_1}\right)}{2\pi} \quad (3.7)$$

D. Application to Fast-Transient Lightning Data Away From Source Region (South Baldy Peak)

These sensors have been successfully employed to obtain high resolution (10 ns) of the electromagnetic fields away from the lightning arcs and corona [15], [16]. The measurements are made at the center of a 30 m \times 30 m square wire-mesh ground plane placed on a relatively flat surface of the earth near the crest of South Baldy Peak in the Magdalena Mountains near Socorro, NM. Copper ground rods are connected at 3-m intervals around the perimeter of the wire mesh and across its surface. The instrumentation room (Kiva) is buried at the center of the wire mesh with its roof flush with the earth and electrically connected to the mesh. Fig. 12 shows the site viewed from the approximate south. The curvature of the mountaintop distorts the low-frequency electromagnetic-field distribution, giving some inaccuracies below about half a megahertz. It is difficult to estimate the quality of the perimeter grounding of the ground plane as no resonance effect is apparent in the data; typical ground impedances indicate accurate performance in the megahertz range and higher. Use of the fast transients of concern [15], [16] in determining direction to the lightning source agrees well with acoustic data, thereby indicating accurate measurements out to at least a few hundreds of nanoseconds on individual pulses.

The Kiva is a 4.25-m diameter by 2.44-m high welded tank made from 3-mm (1/8-in)-thick sheet steel. The top of the tank is extended about 1 m in radius to provide an adequate mounting surface for the sensors, as well as an access area for some of the penetrations into the Kiva. Access to the Kiva is by the stairway shown in the right of the photo. Shielding

integrity of the Kiva is maintained by a "shielded-room" door on the side of the tank.

Two MGL-3 *B*-dot sensors are shown in Fig. 12. The MGL-3 has an equivalent area of 0.1 m². The sensor (*B*-dot east) on the upper portion of the Kiva has its area vector pointing east and the sensor (*B*-dot north) on the left of the Kiva has its area vector pointing north. *B*-dot east has the significance that when *B*-dot is positive in the east direction, the voltage on the center conductor of the sensor output connector is positive, and similarly for *B*-dot north.

The ACD-5 *D*-dot sensor is shown at the front and center of Fig. 12. The area vector for the ACD-5 is pointing toward zenith. A *D*-dot signal that is positive toward zenith will produce a negative voltage on the center conductor of the sensor output connector. These sensors are illustrated in Fig. 8 and 6, respectively, and are discussed in previous subsections.

Each sensor is mechanically and electrically connected to the Kiva surface in several places around the edge of the sensor baseplate. The output signal from each sensor penetrates the Kiva top surface by going directly from the sensor output to a feedthrough connector. RG-213 coaxial cable is used inside the Kiva. The sensors are mounted on a 1.7-m radius about the center of the Kiva. Because of the separation of the sensors, arrival times for signals can vary by up to 11 ns, depending on the azimuth and elevation of the signal source.

Each of the sensor signals is digitized with a Biomation model 8100 waveform recorder. This waveform recorder has 8-bit resolution (256 levels) Each sampled voltage is accurate to 0.4 percent of full scale. The minimum sample interval is 10 ns. The pretrigger mode of recording is used to permit any desired part of the 2048 recorded samples to be those taken before the recorders are triggered. Typically about 20 percent of the samples are saved prior to trigger. The recorders are connected with their triggers in parallel. Triggering any recorder by a signal causes all of them to trigger.

The recorders are controlled by one HP 9825 minicomputer controller. Upon completion of the recorder digitization,

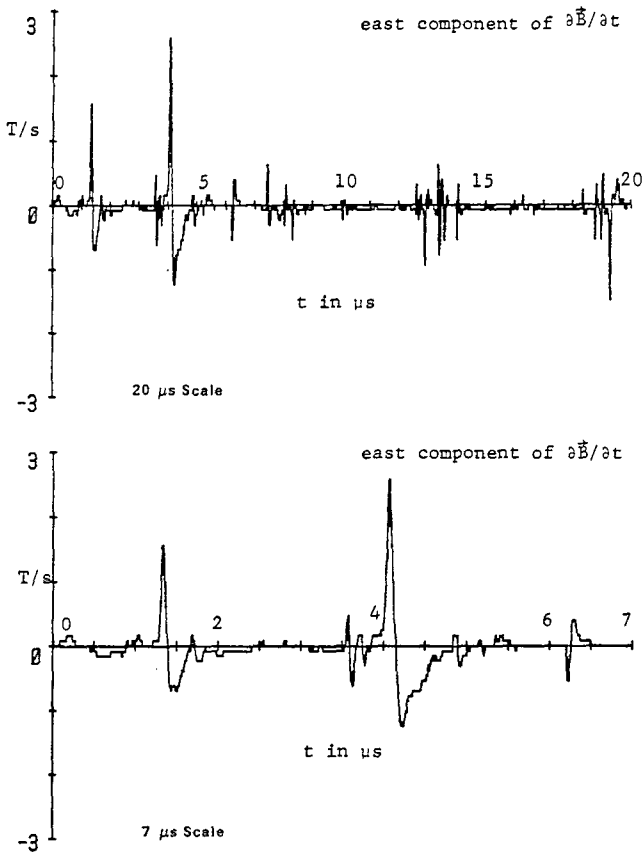


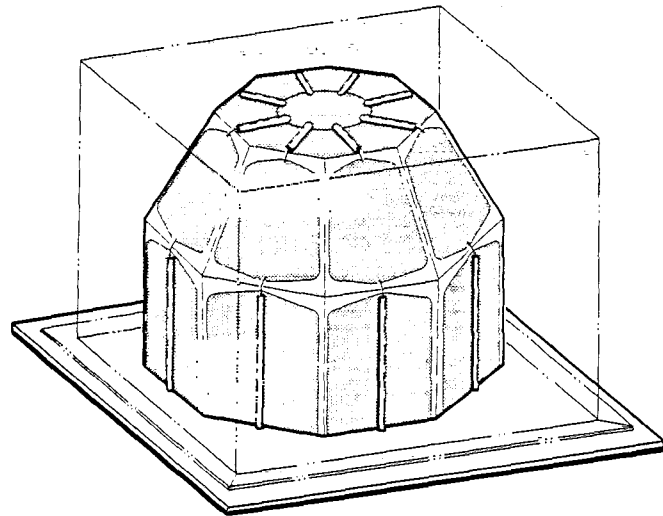
Fig. 13. Leader example.

a signal is sent to the HP 9825 that then transfers the shift-register data from each recorder, in turn, into the memory of the HP 9825. The HP 9825 then rearms the recorders in preparation for acquisition of the next signals. If the recorders are triggered within a certain waiting time, the transfer process is repeated and the recorders are rearmed. This process can be repeated several times, depending on the size of the HP 9825 memory. When the waiting time is exceeded without a recorder trigger, the HP 9825 data are transferred to magnetic disc for later analysis. In this mode of operation, an interval of about 25 ms is required to collect a set of data from the four recorders and then to rearm them for a subsequent acquisition from the same lightning flash. By operating in this mode, it is, in principle, possible to obtain data both on the initiating stepped-leader process and on subsequent return strokes, all in the same flash.

The field information for lightning is obtained by numerically integrating the digitized time-derivative data. The baseline drift of the recorder and the inability to determine accurately the value of the drift results in a ramp error. This problem can be alleviated by integrating the waveforms before sampling.

A timing mark is superimposed on the field-change data to determine where in the lightning-discharge process the fast-waveform recorders are triggered. This is done by triggering a one-shot of about 0.4 s duration from the parallel trigger connection of the Biomation 8100.

Fig. 13 shows an example of the data obtained. On the 20-

Fig. 14. 8AL-1A time-of-arrival B -dot sensor.

μ s scale there are many pulses crowded together. Expanding the first 7 μ s shows some of the wealth of detail in this leader-like data sample. In particular, one begins to get some appreciation of the very fast times involved in such transients and why fast sensors and recorders are required to measure them. This measurement system has found characteristic times for rises even less than 30 ns [15], [16].

As discussed in [15] the transient waveforms from the three sensors can be used to determine the direction of incidence and polarization of the wave, and thereby locate the source when used with acoustic data. They give some information concerning the direction and strength of the source currents. To compare to this, a time-of-arrival system has been installed using three 8AL-1A sensors at approximately the corners of an equilateral triangle with about 92 m edges. Results are currently being obtained.

The 8AL (8-axis loop) is designed to measure the time of arrival of transient electromagnetic signals without regard to the polarization or direction of incidence of the signals. It consists of four loop structures with octagonal symmetry (Fig. 14), with each loop actually forming a double loop structure. A diode network rectifies all signals generated in the loops and drives an impedance-matching transformer at the output connector. The area of each of the eight loops of the 8AL-1A is approximately 0.2 m², but the equivalent area is reduced somewhat by interference from the other loop conductors and by the transformers. The 8AL is not a sensor in the strict sense (see Section II), since it is not intended to measure the fields accurately, but to generate a timing signal based on field arrival time. The effective L/R response time is estimated at about 7 ns.

IV. SENSORS FOR USE NEAR LIGHTNING ARCS AND IN CORONA

The environment inside the lightning arc and corona region is rather inhospitable for electromagnetic measurements. It differs from the nuclear source region in that we do not have a distributed-source current density originating from Compton scatter of γ -rays and photoelectric scatter of X-rays

occurring in air and in the various materials of the sensor itself. We do have conduction effects associated with the surrounding air medium. The impact of the air conductivity is fundamentally different for electric (capacitive-conductive) and magnetic (inductive) devices. Since the air conductivity is a nonlinear effect (because of the dependence of the electron mobility on the electric field), it is imperative that an electric-type sensor not significantly distort the local electric field so as not to change the conductivity. For a magnetic-type sensor, the problem is somewhat different. Local changes in the air conductivity are not as significant; the magnetic field incident on the sensor is more governed by the currents in a volume of space with dimensions of the order of the radian wavelength (or skin depth) so that the local perturbations do not matter so much (at least for the lower frequencies).

The problem of concern, then, is ionization of air, if present, which constrains electric sensor design to be non-distorting of the local electric field, and which loads the loop-gaps of magnetic sensors.

In reducing the deleterious effects in the lightning-source-region, various general guidelines are useful.

1) *For Magnetic Sensor:* The gaps are encapsulated in dielectric to prevent a shunt conductance across the gap.

2) *For Electric Sensor or Current Density Normal to a Conducting Surface:* They must negligibly distort the electric field in the immediate vicinity to not perturb (significantly) the conduction current density.

Various designs of sensors for electric and magnetic fields and currents in lightning source regions have been developed and used and are discussed here.

It is generally easier to construct lightning-source-region sensors than it is to construct nuclear-source-region sensors. The latter source is rich in high-energy photons (γ - and X-ray) and also possibly neutrons. This necessitates sensor elements being as sparse as possible and also that all materials used be of as low atomic number as practical so that cross sections to the irradiation are minimized. This also includes such items as output cables which are specially fabricated and delicate. For lightning sensors, we can use other materials such as brass sheet metal and copper-jacketed coaxial cables.

For mounting of lightning-source-region sensors on objects, such as airplanes, a few simple precautions are in order. The sensors should be as flush with the surface of the object as possible so as not to perturb the fields and possibly attract direct attachment to the sensors. Cables between sensors and recording equipment should be shielded as close to sensors as possible, and the recording system enclosed inside a topological electromagnetic shield. Again, consult the references of [1]-[3] for more details.

A. Electric-Field Sensors

As discussed in the previous section, the most severe effect of a lightning-source environment on electromagnetic measurements is that on the electric-field sensor in air. Effects associated with air conductivity alter the characteristic response of the sensor.

1) *Parallel-Mesh Dipole (PMD):* The parallel-mesh dipole



Fig. 15. Parallel-mesh dipole (PMD-1A) E -field sensor.

sensor, Fig. 15, reduces the effect of the air conductivity by means of having its sensing element constructed of fine wires as opposed to a solid plate of a parallel-plate dipole, so that most of the conduction current is allowed to flow around the dipole conductors instead of through them. The mesh wire is suspended from nylon thread 0.5 cm above the ground plane. In the quasi-static case, the wire grid lies on an equipotential plane, so that the equivalent length of the sensor is also 0.5 cm. The output voltage of the E -field sensor is obtained by measuring, through a sensing resistor, the voltages across the capacitor/conductor formed by the wire mesh and the ground plane. The sensing resistor is in series with the terminated signal cable forming a resistive voltage divider. The voltage across the capacitor will decay with a time constant determined by the sensor capacity and the sensing resistor, except for local conductivity. This time constant must be long compared to measurement times of interest. Note that the PMD-1 is not designed to be mounted on an aircraft where a large air velocity would severely damage it.

B. B-dot and H-Field Sensors

The maximum air conductivity limits the loop radius to the order of a skin depth, or less, at the highest frequency of interest. Below this frequency, the air conductivity does not significantly enter into the loop response. Thus for such a loop the nonlinear and time-varying character of the air conductivity is insignificant. However, sensor-associated equipment such as cables in the air medium should generally be limited to the same dimensions to avoid magnetic-field distortions which may couple into the loop. It is possible to minimize the conductivity-related effects by the use of insulators within the loop structure. Also, the cable impedance which loads the loop can be chosen, together with the loop inductance, to give a frequency response of the order of the skin-depth limitation. The problem of air conductivity is greatly reduced in these sensors by encapsulating the volume enclosing the sensing-element gap with an epoxy resin.

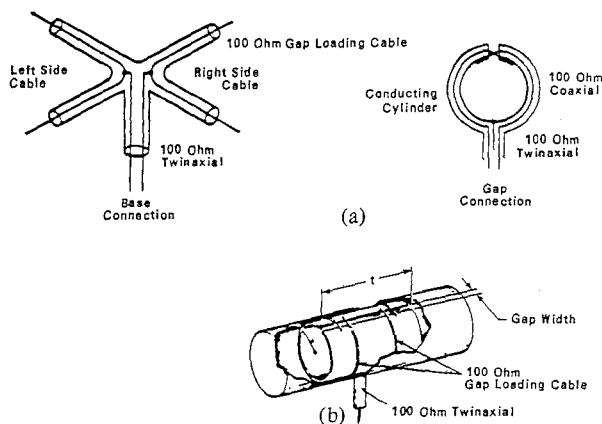


Fig. 16. Cylindrical moebius-loop sensor CML-2B(R). (a) Electrical connections. (b) Typical loop configuration.

1) *Cylindrical Moebius Loop (CML)*: A useful magnetic-field sensor for lightning-source environments is a loop structure with the signal cables wired in a Moebius configuration designated as a cylindrical Moebius loop (CML) sensor. This greatly reduces the common-mode radiation noise currents found in the split-shield-loop type of sensors. A CML sensor can be shown to be a two-turn loop by tracking current flow from one twinaxial cable lead to the other (Fig. 16). At frequencies where the magnetic field does not penetrate the shield of the gap-loading cables, the sensor acts as a single-turn cylindrical loop with a resistive gap load given by the total terminating cable impedance. The four gap-loading coaxial cables in the sensor are properly terminated at the point of coax-to-twinax junction as depicted in Fig. 16. A voltage V at the gap appears as a positive signal in one pair of 100- Ω gap-loading cables and as a negative signal in the other pair. The signal from the gap arrives at the coax-to-twinax junction at the same time from all four gap cables, which produces a differential mode signal across the balanced twinax. For a differential signal, the twinax may be considered to be two resistors, each of a value of 50 Ω to ground, that properly terminate the 50- Ω parallel combination of the two 100- Ω coaxial cables (from each side of the gap). For a given gap voltage, a signal voltage of twice the amplitude of the gap voltage appears at the balanced twinax output.

Several models of CML sensors have been designed and fabricated. They vary in equivalent area from $5 \times 10^{-3} \text{ m}^2$ to 0.02 m^2 , and have been built with encapsulation for use in conductive air measurements.

2) *Multiturn Hardened Loop (MHL)*: Corresponding to the multiturn loop (MTL) designs discussed in the previous section, some similar designs have been built with dielectric encapsulation to avoid the conductivity effects. Designated the multiturn hardened loop (MHL), some designs have already been used for EMP source-region experiments and could be used for lightning experiments.

C. Current and Current-Density Sensors

Radiation-hardened current sensors have been designed which are similar to the CPM series of I -dot probes. These

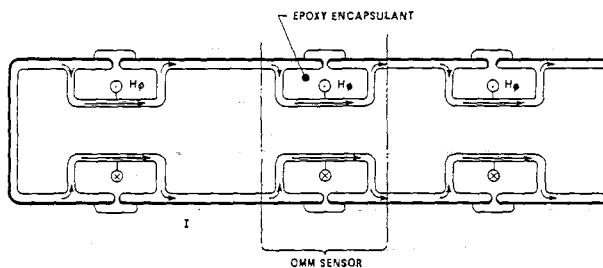


Fig. 17. OMM-1A sensor details.

sensors are designed to be part of a specific structure in a way that they will not appreciably affect the current flow on that structure.

1) *Outside Moebius Mutual Inductance (OMM)*: Fig. 17 shows three OMM-1A I -dot sensors assembled into a cylindrical antenna. Surface current flowing along the cylinder axis must pass through the sensor's internal cavity. The changing magnetic field produced within the sensor cavity produces a voltage across the gap according to $(1/N)MdI/dt$ where M is determined by (3.7). The signal is taken from the gap by four 100- Ω cables in the same manner as shown in Fig. 16 for the CML sensor. The signal cables are routed to the inside of the sensor for electrical purposes and radiation shielding. The sensor interior and gap are encapsulated with an epoxy material in much the same way as with the CML B -dot sensor. The differential signal from each sensor is transmitted by cables of equal length. The OMM-1A has a mutual inductance of $2 \times 10^{-9} \text{ H}$ and a 10-90-rise time $< 0.5 \text{ ns}$. It is 6.4-cm long and of a diameter for use with a 10-cm pipe (outside diameter). A much smaller OMM-2 sensor has been built to measure current in cable shields, conductors, or structural members. It has a mutual inductance of $2 \times 10^{-9} \text{ H}$ and a rise time of $< 0.5 \text{ ns}$. It is 8.9-cm long and designed to use with a 2-cm pipe (outside diameter).

2) *Outside Core I (OCI)*: Similar to the OMM, except using a magnetic core in the toroidal volume for the measured magnetic flux, is the OCI. This arrangement makes the output respond to the current waveform instead of its time derivative above some low frequency. Multiturn windings with coaxial cables and Moebius gaps are also used, thereby employing many of the design features of the multiturn hardened loops (MHL). These sensors have been used in nuclear source regions and are applicable to lightning. One should be careful of the large low-frequency content of lightning return-stroke pulses and the corresponding possibility of unwanted saturation of the magnetic cores.

3) *Flush-Plate Dipole (FPD)*: Special FPD-2 sensors have been made for aircraft flying in lightning source regions (direct stroke attachment); their sensitivity is $A_{eq} = 0.02 \text{ m}^2$. The performance of these FPD sensors was necessarily degraded from that of the standard FPD in the following areas. The distance between the sensing element and the bottom pan was reduced because of size limitation on the sensor location. The volume between the element and the pan was filled with dielectric both to eliminate the possibility of conductive air within the sensor and to provide a firm mounting for the element in the aircraft windstream. The gap area was also thor-

oughly encapsulated with dielectric. All of the above steps serve to increase the sensor capacitance with the result that the bandwidth is decreased to 70 MHz. Versions of this hardened sensor were also made with rectangular sensing elements to fit specified areas. Both circular and rectangular versions were made with curved surfaces, including the sensing element, to conform to the aircraft shape so as to not create either electrical or airflow protuberances. The figure of merit for these special FPD sensors is thereby reduced to 0.005.

4) *Flush Moebius Mutual Inductance (FMM)*: With external geometry similar to the FPD, the FMM has been used in nuclear source regions because of its low impedance (a small inductance) loading the central plate. The signal pickoff is like the OMM, to which the response is similar. This sensor responds to the time derivative of the total current, thereby emphasizing the high frequencies.

D. Lightning Environmental Measurements on Aircraft

In order to define lightning environmental criteria for aircraft, appropriate to the vulnerability of the electronics, one needs measurements of the lightning environment under in-flight conditions. This raises the question of how to perform such measurements and which measurements are most appropriate. Two situations are of interest: a near miss and (more important) a direct strike.

For the case of a near miss (say hundreds of meters or somewhat larger) one can first use data available from measurements on the ground. For the important fast transients as in [13], [15], the fields can be extrapolated back to the sources and fields closer to the source using the Green's-function techniques in [15].

On an aircraft, one can, in principle, measure the electromagnetic fields incident on the aircraft. However, such measurements are very difficult due to the aircraft scattering. If one places sensors on the aircraft skin or near it, one must recognize that, in general, the aircraft is now part of the sensor and introduces the aircraft resonances into the sensor response. These can introduce errors which vary the response by an order of magnitude over the frequencies of concern. Furthermore, this wild response varies strongly with angle of incidence and polarization of the incident wave. Unfolding the true incident fields is a difficult inverse-scattering problem. In such a measurement, one has the surface fields (or surface current and charge densities) for a particular airplane which cannot be directly applied to another airplane. This situation leads to surface electromagnetic parameter measurement on many aircraft. A similar, but even more complex, problem occurs if one measures the internal response at selected points on a particular aircraft.

If one wishes to measure the fields incident on an aircraft, then one must be very careful how he goes about it. Specifically, one should find spatial locations with respect to the aircraft such that the aircraft scattering can be neglected, at least for particular field components. Most aircraft have an electromagnetic symmetry plane (as far as external scattering is concerned) passing through the fuselage from nose to tail and approximately perpendicular to the wings. Incident and scattered fields can be divided into two independent parts

designated symmetric and antisymmetric with respect to this symmetry plane [3], [24]. Placing a magnetic sensor on this plane for measuring a magnetic field parallel to the plane makes it totally insensitive to the symmetric scattering (which includes the large fuselage resonances). Rotating the sensor axis one can try to cross polarize it to the antisymmetric scattering from say the wings and horizontal stabilizers (if present); for this purpose, the wings and horizontal stabilizers should be in the same direction from the sensor. This places the sensor off the nose or tail of the aircraft. Selecting, say, the nose to avoid the close proximity of the horizontal stabilizers, one can construct a conducting boom (which can shield the sensor cable(s)) protruding from the nose a fuselage diameter or two to minimize the local antisymmetric magnetic field scattered from the fuselage. This is not an easy measurement. Alternatively, one might have a boom or trailing package extended sufficiently far from the tail. One might also begin by orienting the sensor to be insensitive to the antisymmetric scattering leading to similar conclusions concerning sensor location.

In a direct-strike situation, one cannot separate incident and scattered fields due to the nonlinear arc and corona processes. One is forced to measure surface electromagnetic parameters, and hence to measure these on various aircraft. One would like at least to bound these electromagnetic parameters for various aircraft skin locations to be able to apply the results, at least approximately, to new untested aircraft designs. The sensors discussed in this section are appropriate for these measurements. Since one is usually limited as to number of waveform measurements on a particular aircraft, then one must be concerned with where to place the sensors. Total-normal-current-density sensors (as well as electric-field sensors) would first be placed near the aircraft extremities (nose, tail, and wing tips) where such fields are intense. Magnetic sensors could be placed near the wing/fuselage intersection through which the currents from the lightning arcs (which tend to attach/detach near the extremities) will pass, noting that the currents into such a junction approximately sum to zero (Kirchoff approximation). Current sensors can be built into likely extended attachment/detachment positions such as the pitot tube.

Note that, even in direct-strike conditions, one can at least approximately separate the exterior aircraft response from the interior response if the skin has some shielding properties. The exterior region as well as some of the penetrations will be affected by the nonlinear corona [23]. It is these aspects that require special measurements. The response of the aircraft interior can be considered somewhat separately using concepts from electromagnetic topology [25].

E. WC-130 Experiments

A joint program with the Air Force Wright Aeronautical Laboratories and the National Oceanic and Atmospheric Administration has instrumented a WC-130 aircraft as indicated in Fig. 18. Some results are given in [17]. Most recently [18], some direct strikes have been obtained.

The latest CML design is specifically intended for skin-current B -dot measurements on aircraft flying in and near thun-

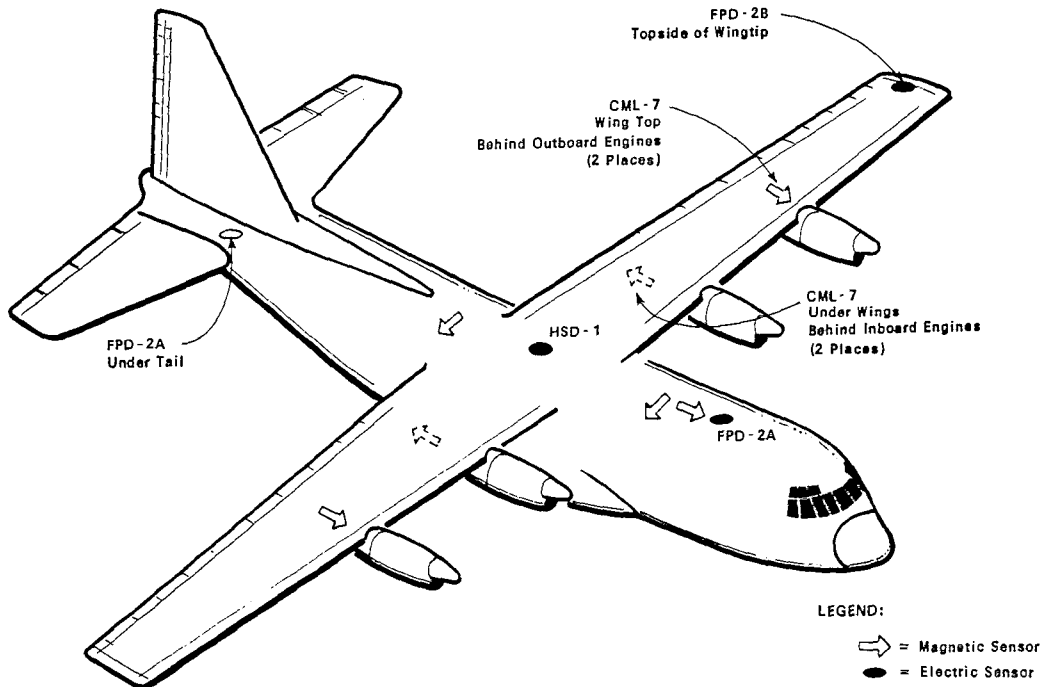


Fig. 18. Sensor locations on WC-130 NOAA aircraft.

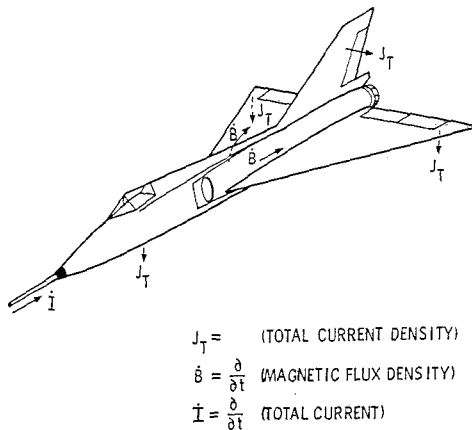


Fig. 19. Sensor locations on NASA F-106 aircraft.

derstorms. The ground plate mounts flush with the aircraft skin as it replaces a patch of skin on an aircraft panel. Fig. 18 shows the sensor locations as used on the NOAA WC-130 aircraft in recent Air Force tests. This CML-7 sensor is not optimized for high-frequency bandwidth, but rather for signal level versus physical size and for aerodynamic consideration. The upper frequency response is about 35 MHz with a 10-ns rise time.

F. F-106 Experiments

A program at NASA, Langley, has recently obtained some data on the surface current density and normal total current density on the skin of a specially instrumented F-106 under direct-strike conditions [21], [22]. A schematic of the aircraft with its measurement locations is given in Fig. 19. For these measurements, a set of special-purpose $\partial \vec{B} / \partial t$, \vec{J}_t , and $\partial I / \partial t$ sensors (noting the nonstandard sensitivities) were fabricated

by NASA following the previously discussed designs [19]. Their parameters are summarized as

Type of Sensor	Quantity Measured	Sensitivity	Rise time (10%-90%)
Multigap Loop	$B\text{-dot}$	$5.73 \times 10^{-3} \text{ m}^2$	0.85 ns^1
Flush-Plate Dipole	J_t	$4.09 \times 10^{-2} \text{ m}^2$	2.4 ns^1
Outside Moebius			
Mutual Inductance	$I\text{-dot}$	$2.13 \times 10^{-9} \text{ H}$	0.23 ns^2

Notes: ¹ Measured.
² Calculated.

To record the transient signals, some of the data channels used specially modified digital recorders for long data records. The transient recorders used in NASA Direct Strike Lightning Research [20] are modified Biomatron Model 6500 Waveform Recorders. The Biomatron 6500 is a fast analog-to-digital converter (ADC) with internal storage for 1024 6-bit words. At the fastest rate, the Biomatron 6500 samples an analog signal every 2 ns and has an input analog bandwidth of 100 MHz. The recorders operate in an "endless loop" mode, wherein the recorder continuously samples and stores data until a trigger event occurs which causes the record phase to end. The recorded data are then read out at a slower rate for permanent storage. Once the memory has been read out, it returns to the record phase to await the next trigger event.

A memory expansion from 1024 to 131 072 samples allows a significantly longer data record than obtainable with the basic unit [20]. For example, the modified recorder can store a 1300- μs "snapshot" of data with a time resolution of 10 ns per data sample. The major characteristics of the modified recorder are storage of 131 072 samples as compared to 1024, increase of memory integrated circuits from 48 to 192, and

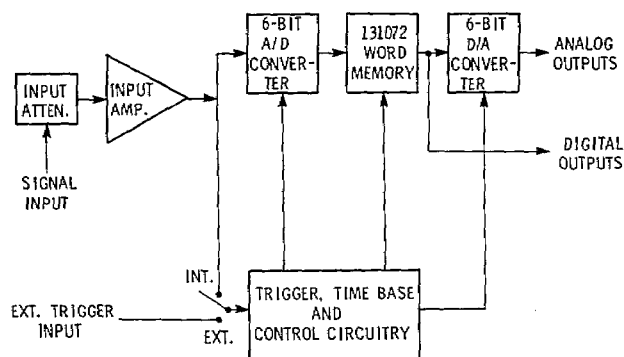


Fig. 20. Schematic of transient recorder.

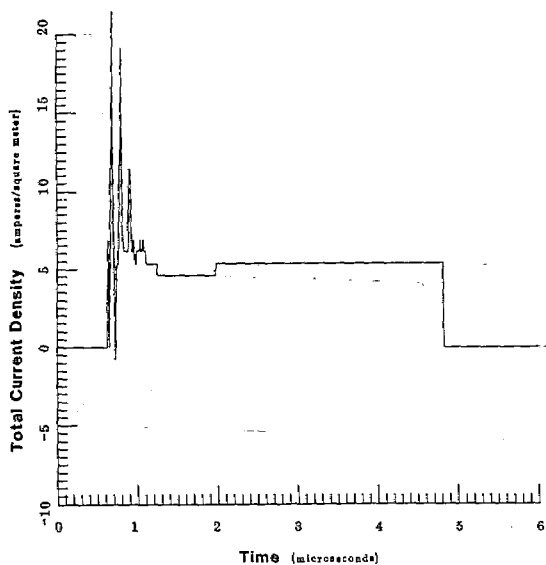


Fig. 21. Example of total current density normal to aircraft skin under direct-strike conditions.

provision for delaying the trigger by up to 100 000 sample intervals.

The major components of the transient recorder are indicated in Fig. 20. The signal to be recorded is presented to the input attenuators and amplifier, digitized, and then stored in the memory. The control circuitry selects the data period to be retained. Once a "snapshot" has been obtained, it is routed to permanent storage via the analog or digital outputs. The Biomation 6500 recorder achieves its high sampling rate by employing a parallel ADC technique. The output of the ADC is converted to a 6-bit gray code. In order to provide more time for the storage of the data, the ADC output is double buffered into two 6-bit registers on an alternating basis. The output of these two registers is presented to the memory board on two 6-bit parallel buses. The expanded memory is partitioned into 32 sections, each employing memory devices which have a 55-ns write-cycle time; the write cycles of the memory devices are overlapped through a series of intermediate registers. The ADC, operating at its designed maximum sample rate, generates a data word every 2 ns. The first data word is routed to the first memory location in memory section one, 2 ns later the second data word is routed to the first memory location in memory section two, and so on until the first 32 data samples have been routed to the 32 memory

sections. The elapsed time of 64 ns allows the first memory device to complete its write cycle (55 ns) in time for the next sequence of data words. Through the use of memory interleaving, an effective speed of 2 ns between samples is thus obtained using memory devices of 55-ns write-cycle time.

While not all the results are in, the early results are quite remarkable. Fig. 21 shows the normal current density (conduction plus displacement with positive polarity outward from the skin) taken below and behind the nose (i.e., the chin) of the F-106 at the position indicated in Fig. 19. Note the early-time resonant behavior with times corresponding to transit times on the aircraft exterior. Note also the continuing current density of $\approx 5 \text{ A/m}^2$ for $\approx 4 \mu\text{s}$. Neglecting corona, this can be integrated to give about 2 MV/m for the change in electric field.

These results point out the significance of electric (as well as magnetic) parameters and high-frequency resonance effects on aircraft, and the necessity for including them in simulation of lightning on aircraft as discussed in a previous paper [23]. Note also the rise times in the 30-ns regime agreeing with the field measurements in [15].

V. SUMMARY

As should be apparent by now, electromagnetic-field measurements can be simple or complex, depending on frequency, sensor size, and other environmental parameters. Obtaining more signal and bandwidth from a sensor and minimizing the influence of adverse environmental conditions is quite possible if one is willing to go beyond the elementary concepts of electrically small electric- and magnetic-dipole antennas in linear, uniform, isotropic media. As discussed in [1]–[3] and their references, there are many design techniques to extend sensor performance.

The phenomenon of lightning and its study have been around for some time, but perhaps they have not had much priority attention, at least insofar as interaction with electronic systems is concerned. Increasing interest in the vulnerability of electronic systems to lightning transients is perhaps related to the increased dependence of systems on more and more sensitive electronics. The important role of the fast-transient character of the lightning waveforms in the interaction of lightning with electronic systems has made it imperative to measure the appropriate electromagnetic waveforms with accurate, large-bandwidth sensors and associated instrumentation. The technology from EMP is now, fortunately, being applied to the problem; this gives good promise for the future.

ACKNOWLEDGMENT

We would like to thank Dr. Krider and Dr. Uman for their assistance in obtaining and selecting some of these older references.

REFERENCES

- [1] C. E. Baum, E. L. Breen, J. C. Giles, J. P. O'Neill, and G. D. Sower, "Sensors for electromagnetic pulse measurements both

- inside and away from nuclear source regions," *Sensor and Simulation*, note 239, Jan. 1978, *IEEE Trans. Antenna Propagat.*, Jan. 1978, pp. 22-35, and *IEEE Trans. Electromag. Comput.*, Feb. 1978, pp. 22-35.
- [2] C. E. Baum, E. L. Breen, C. B. Moore, J. P. O'Neill, and G. D. Sower, "Electromagnetic sensors for general lightning application," in *Proc. Lightning Tech.*, NASA Conf. Pub. 2128 and FAA-RD-80-30, Apr. 1980, pp. 85-118.
- [3] C. E. Baum, "Sensors for measurement of intense electromagnetic pulses," *Sensor and Simulator Note 271*, June 1981, and in *Proc. 3rd IEEE Int. Pulsed Power Conference*, Albuquerque, NM, June 1981.
- [4] E. V. Appleton, R. A. W. Watt, and J. P. Herd, "On the nature of atmospherics II," in *Proc. Royal Society, A*, vol. III, p. 616 ff, 1923.
- [5] H. Norinder, "Rapid variations in the magnetic field produced by lightning discharges," in *Proc. Phys. Soc. London*, vol. 49, p. 365 ff, 1937.
- [6] N. Kitagawa and M. Brook, "A comparison of intracloud and cloud-to-ground lightning discharges," *J. Geophys. Res.*, vol. 65, Apr. 1960, pp. 1189-1201.
- [7] R. J. Fisher and M. A. Uman, "Measured electric field risetimes for first and subsequent lightning return strokes," *J. Geophys. Res.*, vol. 77, Jan 20, 1972, pp. 399-406.
- [8] E. P. Krider and R. C. Noggle, "Broadband antenna systems for lightning magnetic fields," *J. Appl. Meteorol.*, vol. 14, no. 2, Mar. 1975, pp. 252-256.
- [9] E. P. Krider, R. C. Noggle, and M. A. Uman, "A gated, wideband magnetic direction finder for lightning return strokes," *J. Appl. Meteorol.*, vol. 15, no. 3, Mar. 1976, pp. 302-306.
- [10] E. P. Krider, C. D. Weidman, and R. C. Noggle, "The electric fields produced by lightning stepped leaders," *J. Geophys. Res.*, vol. 82, no. 6, Feb. 20, 1977, pp. 951-960.
- [11] C. D. Weidman and E. P. Krider, "The fine structure of lightning return stroke waveforms," *J. Geophys. Res.*, vol. 83, No. C12, Dec. 20, 1978, pp. 6239-6247.
- [12] E. P. Krider, R. C. Noggle, A. E. Pifer, and D. L. Vance, "Lightning direction-finding systems for forest fire detection," *Bull. Amer. Meteorol. Soc.*, vol. 61, no. 9, Sept. 1980, pp. 980-986.
- [13] D. C. Weidman and E. P. Krider, "Submicrosecond risetimes in lightning radiation fields," *Proc. Lightning Tech.*, NASA Conf. Pub. 2128, and FAA-RD-80-30, Apr. 1980, pp. 29-38, also as "Submicrosecond risetimes in lightning return-stroke fields," *Geophys. Res. Lett.*, vol. 7, no. 11, Nov. 1980, pp. 955-958.
- [14] E. P. Krider, private communication.
- [15] C. E. Baum, E. L. Breen, D. L. Hall, C. B. Moore, and J. P. O'Neill, "Measurement of electromagnetic properties of lightning with 10 nanosecond resolution," *Proc. Lightning Tech.*, NASA Conf. Pub. 2128 and FAA-RD-80-30, Apr. 1980, pp. 39-82.
- [16] C. E. Baum, "Electromagnetic characterization of lightning in the submicrosecond regime," *URSI XXth Gen. Assembly*, Wash., D.C. Aug. 1981.
- [17] R. K. Baum, "Airborne lightning characterization," in *Proc. Lightning Tech.*, NASA Conf. Pub. 2128 and FAA-RD-80-30, Apr. 1980, Supplement pp. 1-20.
- [18] G. Dubro, private communication.
- [19] T. F. Trost and K. P. Zaepfel, "Broadband electromagnetic sensors for aircraft lightning research," *NASA Conf. Pub. 2128 and FAA-RD-80-30*, Apr. 1980, pp. 131-152.
- [20] R. M. Thomas, Jr., "Expanded interleaved solid-state memory for a wide bandwidth transient waveform recorder," *NASA Conf. Pub. 2128 and FAA-RD-80-30*, Apr. 1980, pp. 119-129.
- [21] F. L. Pitts and M. E. Thomas, "1980 direct strike lightning data," *NASA Tech. Memo 81946*, Feb. 1981.
- [22] F. L. Pitts, "Electromagnetic measurement of lightning strikes to aircraft," *AIAA Paper 81-0083*, Jan. 1981.
- [23] C. E. Baum, "Simulation of electromagnetic aspects of lightning," *Proc. Lightning Tech.*, NASA Conf. Pub. 2128 and FAA-RD-80-30, Apr. 1980, pp. 283-299.
- [24] C. E. Baum, "Interaction of electromagnetic fields with an object which has an electromagnetic symmetry plane," *Interaction Note 63*, Mar. 1971.
- [25] C. E. Baum, "Electromagnetic topology: A formal approach to the analysis and design of complex electronic systems," *Interaction Note 400*, Sept. 1980.